Symmetry and the critical slip distance in rate and state friction laws

Andrew P. Rathbun[1,2,3] and Chris Marone[2,3]

Received 12 May 2012; revised 5 December 2013; accepted 19 May 2013.

[1] We performed laboratory experiments to investigate the processes responsible for rate and state friction (RSF) behavior in fault rocks. We focused on the symmetry of the frictional constitutive response to velocity changes and the mechanics of the critical friction slip distance D_c. Experiments were conducted in double direct shear at 1 and 25 MPa normal stress, at room temperature, and for shearing velocity from 1 to 300 μm/s. We studied three granular materials and bare surfaces of Westerly granite. Ruina's law, which predicts frictional symmetry between velocity increases and decreases, better matches our data than Dieterich's law, which predicts that velocity decreases should evolve to steady state at a smaller displacement. However, for granular shear, in some cases D_c is smaller for velocity increases than for velocity decreases, contrary to expectations from either law. On bare granite surfaces, the frictional response is symmetric for velocity increases/decreases. Two distinct length scales for D_c and two-state variables are required for granular shear in some cases. We hypothesize that asymmetry and two-state behavior are caused by shear localization and changes in shear fabric in fault gouge. Our measurements show that during steady state frictional shear, dilation after a velocity increase is smaller than compaction after a decrease. Normal stress oscillations cause a marked decrease in D_c. Reduction of D_c reduces frictional stability, enhancing the possibility of seismic slip. Our experiments show that shear localization and fabric within the fault gouge can influence the RSF parameters that dictate earthquake nucleation and dynamic rupture.

Citation: Rathbun, A. P., and C. Marone (2013), Symmetry and the critical slip distance in rate and state friction laws, *J. Geophys. Res. Solid Earth*, *118*, doi:10.1002/jgrb.50224.

1. Introduction

[2] Earthquakes in the brittle crust are controlled by frictional processes [e.g., *Scholz*, 2002], and observations from both exhumed faults [e.g., *Logan et al*., 1979; *Chester and Chester*, 1998; *Cashman and Cashman*, 2000; *Faulkner et al*., 2003; *Hayman et al*., 2004; *Cashman et al*., 2007] and faults at depth [*Zoback et al*., 2010] indicate that gouge zones play a key role in determining fault stability and slip behavior. Fault gouge is typically unconsolidated near Earth's surface, with the degree of lithification increasing with depth. The fault gouge in tectonic fault zones can range in thickness from centimeters to tens of meters [*Scholz*, 2002; *Sibson*, 2003].

[3] Typically, brittle faulting is described using rate and state friction (RSF) laws [*Dieterich*, 1979; 1981; *Ruina*, 1983]. In these empirical relations, second-order friction variations are described in terms of slip velocity and a state variable, which can be related to the average lifetime of asperity contact junctions [e.g., *Rabinowicz*, 1958] and the porosity of granular materials [*Marone et al*., 1990; *Segall and Rice*, 1995]. Previous studies show that friction of the fault gouge depends on asperity contact processes and also granular processes and effects arising from clay particles and shear fabric [e.g., *Marone*, 1998; *Niemeijer et al*., 2010; *Ikari et al*., 2011; *Faulkner et al*., 2011; *Tesei et al*., 2012]. These processes can result in a range of friction behaviors, and two classes of RSF laws have been proposed to describe laboratory data and earthquake rupture. The majority of existing laboratory data are incapable of distinguishing between RSF laws; however, theoretical studies predict important differences in earthquake nucleation and the characteristics of dynamic rupture depending on the RSF law [e.g., *Heaton*, 1990; *Rice*, 1993; *Rubin and Ampuero*, 2005; *Ampuero and Rubin*, 2008].

[4] While similar in form, the two basic state evolution laws yield significantly different predictions of seismic behavior and earthquake rupture nucleation [i.e., *Rubin and Ampuero*, 2005; *Bayart et al*., 2006; *Ampuero and Rubin*, 2008]. Several investigators have noted that numerical models of stick-slip and dynamic rupture propagation only reproduce Gutenberg-Richter frequency-magnitude phenomena and the slip pulse mode of rupture when Dieterich's law

[1]Institut des Sciences de la Terre, Université Joseph Fourier - Grenoble 1 and CRNS/OSUG, Grenoble, France.
[2]Department of Geosciences, Pennsylvania State University, University Park, Pennsylvania, USA.
[3]Sediment and Rock Mechanics Laboratory, Pennsylvania State University, University Park, Pennsylvania, USA.

Corresponding author: A. P. Rathbun, Institut des Sciences de la Terre, Université Joseph Fourier - Grenoble 1 and CRNS/OSUG, BP 53, FR-38041 Grenoble, France. (andrew.rathbun@ujf-grenoble.fr)

2169-9313/13/10.1002/jgrb.50224

is used [e.g., *Heaton*, 1990; *Rice*, 1993; *Perrin et al*., 1995; *Beeler and Tullis*, 1996]. *Ampuero and Rubin* [2008] found that the rupture nucleation length varies considerably depending on which law is used. They showed that the nucleation zone for Dieterich's law should approach ~1 km, while the predicted nucleation zone for Ruina's law is ~100 times smaller. The recent models of *Kaneko and Ampuero* [2011] recreate slow rupture fronts observed in laboratory experiments [*Nielsen et al*., 2010] with both common state evolution laws but with different parameters depending on which law is used.

[5] The purpose of this study is to investigate the two classes of RSF behavior. We focus in particular on the frictional response to velocity step tests and compare results for increases and decreases in velocity, which is a discriminant for the two classes of RSF laws. We investigate shear in granular layers and between bare rock surfaces and compare responses for both large and small velocity steps. Our experimental velocities were chosen to address the nucleation phase of dynamic rupture and the velocities at which faults slip in the mid to later stages of postseismic deformation. We were also motivated by the fact that this velocity range has been used extensively in previous studies; thus, we chose it for ease of comparison with these existing studies.

1.1. Rate and State Friction Laws: Which Class of State Evolution?

[6] In its simplest form, the RSF equation is expressed as

$$\mu(V,\theta) = \mu_0 + a\ln\left(\frac{V}{V_0}\right) + b_i \ln\left(\frac{V_0\theta_i}{D_{ci}}\right) \quad (i = 1,2) \quad (1)$$

where μ is sliding friction at velocity V and μ_0 is sliding friction at reference velocity V_0. The constitutive constant, a, often referred to as the direct effect, is thought to be the result of Arrhenius processes resulting from breaking bonds at the atomic level [e.g., *Rice et al*., 2001]. The friction evolution effect, b, describes changes in friction with time and slip over a critical length scale, D_c. The lifetime of frictional contacts is given by the ratio of contact size to slip velocity, which can be described by the friction state variable, θ, which has units of time. Equation (1) can be written in terms of one or more state variables, each with a distinct length scale, D_c. In most cases, only one length scale is considered and b_2 is taken to be 0. We consider both one-state variable behavior and two-state variable behavior in the analysis below.

[7] The RSF relation (1) is coupled with a second equation describing the evolution of the state variable. Typically, one of two common evolution laws is used:

$$\textit{Dieterich's ``aging'' law}: \quad \frac{d\theta_i}{dt} = 1 - \frac{V\theta_i}{D_{ci}} \quad (i = 1,2) \quad (2)$$

$$\textit{Ruina's ``slip'' law}: \quad \frac{d\theta_i}{dt} = -\frac{V\theta_i}{D_{ci}}\ln\left(\frac{V\theta_i}{D_{ci}}\right) \quad (i = 1,2) \quad (3)$$

[8] These laws differ in their behavior at $V = 0$. Dieterich's aging law (hereafter referred to as Dieterich's law) predicts the evolution of the state variable due to aging at grain-to-grain contacts at zero velocity, while Ruina's slip law (hereafter referred to as Ruina's law) predicts that state evolution requires slip and does not occur at $V = 0$. In the aging law, contact lifetime is the dominant factor, while velocity and slip dictate state evolution.

[9] To predict frictional constitutive behavior, the RSF equations must be coupled with a description of continuum interactions between a fault and its surroundings. Our laboratory experiments are well described as a one-dimensional elastic system [e.g., *Gu et al*., 1984], which can be written as follows:

$$\frac{d\mu}{dt} = k(V_1 - V) \quad (4)$$

where k is the elastic loading stiffness of the apparatus, expressed as frictional shear stress divided by normal stress; V_1 is the load-point velocity; and V is velocity at the slip surface.

[10] Several variants of the two common state evolution laws have been proposed. *Perrin et al*. [1995] proposed a hybrid law that is symmetric for velocity increases/decreases and allows state evolution at zero slip velocity. *Kato and Tullis* [2001] proposed a composite law with a cutoff velocity such that healing occurs even at very low slip velocities. Their law is optimized for numerical modeling of the full stick-slip seismic cycle. To account for quasi-dynamic and other forms of slow fault slip, the state evolution laws have been coupled with pressure changes and dilatancy [e.g., *Segall and Rice*, 1995; *Rubin*, 2008; *Segall et al*., 2010; *Samuelson et al*., 2009, 2011] or modified to include multiple state variables [*Rubin*, 2011]. *Beeler* [2009] modified the state evolution equations to include cutoff velocities appropriate for behavior in the brittle-ductile transition. *Nagata et al*. [2012] discussed technical problems in experiments in which elastic stiffness is low or poorly constrained, allowing significant state evolution during measurement of the friction direct effect.

[11] We focus on RSF behavior following velocity perturbations and use the symmetry of the frictional constitutive response to evaluate state evolution and the mechanics of the critical friction slip distance. Figure 1 compares the two friction state evolution laws for 3X velocity steps and a range of stiffnesses from $k = 0.0005\ \mu m^{-1}$ to the theoretical case of $k = \infty$. In our experiments, $k = 0.001$–$0.002\ \mu m^{-1}$ and is determined from the initial linear portion of the friction-displacement curve after a step change in velocity. Results for step increases in velocity are shown in black in Figure 1. Velocity decreases are shown in red and in inverted form in green for comparison. At low stiffness, the peak friction for velocity increases is markedly higher than that for decreases (Figure 1). Also, pre-peak behavior differs for velocity increases and decreases; velocity decreases require a smaller slip to reach peak friction compared to increases, which is consistent with the higher apparent stiffness expected for velocity decreases when plotted versus load-point displacement. The differences in pre-peak behavior become less pronounced with increased stiffness, with no difference in the case of infinite stiffness. We impose step changes in velocity in order to isolate the two main effects of RSF: the friction direct effect and the state evolution effect. Although this procedure has no direct application to faulting, we note that particles on a fault experience extremely high acceleration as the rupture approaches and passes. Indeed, the particle slip

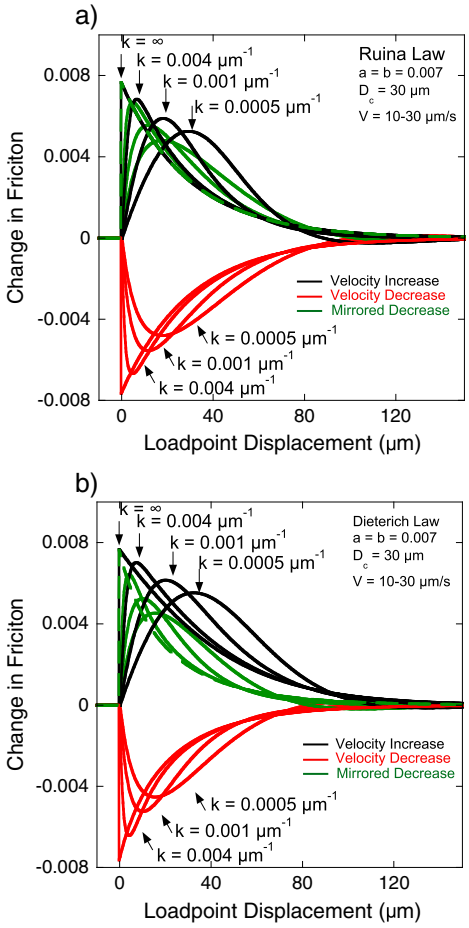

Figure 1. Comparison of (a) Dieterich's law and (b) Ruina's law. Four velocity increases (black) and four decreases (red) are shown for steps between 10 and 30 μm/s. Velocity decreases are flipped and presented as mirror images for comparison to increases (green). Rate and state parameters are $a = b = 0.007$ and $D_c = 30$ μm. Simulations are shown for four values of elastic stiffnesses, cast as shear stress divided by normal stress. The infinitely stiff case is dashed to highlight the identical behavior in Figure 1b.

velocity changes over several orders of magnitude during this process.

[12] The results in Figure 1 show that Dieterich's law predicts asymmetric behavior for velocity increases compared to decreases and that the degree of asymmetry increases as elastic stiffness decreases, consistent with previous work [*Dieterich*, 1979; *Ruina*, 1983; *Rice*, 1983]. The fundamental difference between these state evolution laws lies in the slip required for friction to return to steady state after velocity increases versus decreases. For a range of finite stiffnesses, Dieterich's law (Figure 1a) predicts that friction curves for velocity increases (decreases) will match starting at a displacement of ~110 μm, whereas Ruina's law (Figure 1b) predicts that the curves begin to match at a displacement of ~50 μm. Dieterich's law's prediction of time as the controlling variable in state evolution leads to steady state friction at a smaller relative displacement for velocity decreases versus increases, whereas in Ruina's formulation, slip is the key factor, causing both decreases and increases to reach steady state at equal displacements (Figure 1).

[13] Previous laboratory experiments have been inconclusive in separating which law should be used. Early experiments tended to favor Ruina's law due to its prediction of symmetry between velocity increases and decreases [e.g., *Ruina*, 1983; *Tullis and Weeks*, 1986; *Marone et al*., 1990]. Imaging experiments by *Dieterich and Kilgore* [1994] showed that the real contact area evolved with normal stress and time, favoring Dieterich's law. *Beeler et al*. [1994] performed experiments in which the stiffness of the loading apparatus was varied. They found that Dieterich's law better fit their data over a range of hold times from ~3 to 10^5 s. *Blanpied et al*. [1998] observed a better match with Ruina's law and two-state behavior in both room temperature and experiments up to 800°C. *Bayart et al*. [2006] conducted laboratory experiments on 3 mm thick granular zones and noted symmetric behavior at small step sizes and for steps of up to 3 orders of magnitude, consistent with Ruina's law. Finally, *Noda and Shimamoto* [2010] conducted experiments on halite near the brittle-ductile transition and found that D_c is independent of strain rate over several orders of magnitude.

[14] In low-stress experiments (normal stress equal to 1 MPa) on glacial till, *Rathbun and Marone* [2010] observed that modeling for the RSF parameters yielded a longer D_c for velocity decreases than increases, opposite to predictions of Dieterich's law; hence, they favored the symmetric Ruina law. They proposed an alternative model in which the width of the active shear zone varies with slip velocity and frictional state, as suggested in previous work [e.g., *Marone and Kilgore*, 1993; *Sleep et al*., 2000; *Marone et al*., 2009]. In such a model, interactions between the zone of shear localization and adjacent spectator regions have a separate and important impact on RSF friction, in addition to interparticle contact aging [e.g., *Dieterich*, 1979] and granular porosity [e.g., *Segall and Rice*, 1995]. *Rathbun and Marone* [2010] hypothesized that variations in shear bandwidth were asymmetric for velocity increases and decreases, which leads to differences in the effective critical slip distance.

2. Experimental Methods

[15] Experiments were conducted on three granular materials with varying grain sizes (Figure 2) and bare surfaces of Westerly granite. Two types of granular quartz were obtained from U.S. Silica Company (Rolla, Missouri): (1) medium-grained and subangular pure quartz sand with trade name F110 (hereafter referred to as medium sand) and (2) silt-sized to clay-sized pure quartz powder with trade name Min-U-Sil 40 (hereafter referred to as fine-grained quartz). In addition, we used Caesar till, which is subangular to subrounded, a predominantly coarse grained sand obtained from the former Scioto Lobe of the Laurentide Ice Sheet, and composed of 35% quartz, 26% calcite, 23% plagioclase, and 16% clay minerals, with clay mineral abundances of 35.3% smectite, 38.5% illite, and 26.1% chlorite/kaolinite [*Rathbun et al*., 2008; *Rathbun and Marone*, 2010]. The complete grain size distributions of all three granular materials are shown in Figure 2. For bare surface experiments, samples of Westerly granite were prepared by precision grinding block squares parallel to within 0.001″ over the

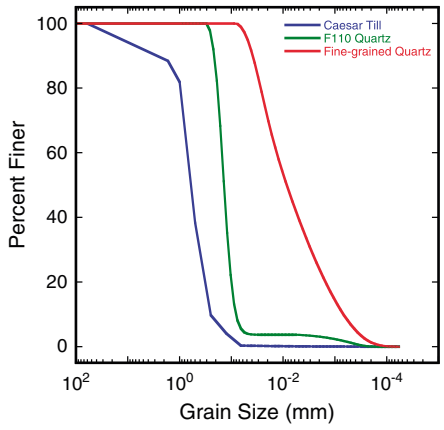

Figure 2. Grain size distribution of the three granular materials used in this study. Grain size is determined via the laser absorption method for medium-sand and fine-grained quartz samples. Caesar till is sieved to 0.064 mm and then measured via laser absorption.

nominal dimensions of 10 cm × 10 cm × 15 cm and then sandblasting the surfaces with #200 grit glass beads to roughen the surfaces.

[16] All experiments were conducted in a servohydraulic testing apparatus in the double direct shear configuration. Our configuration consisted of two parallel shear zones with equal thicknesses and contact areas sandwiched between three steel blocks (Figure 3, inset). The steel forcing blocks were roughened to ensure that the blocks are well coupled to the gouge zone with no boundary shear [e.g., *Rathbun et al*., 2013]. Force was measured via BeCu load cells attached to each loading ram, and displacement was measured external to the shear zone by direct current displacement transducers. Details of the experimental apparatus can

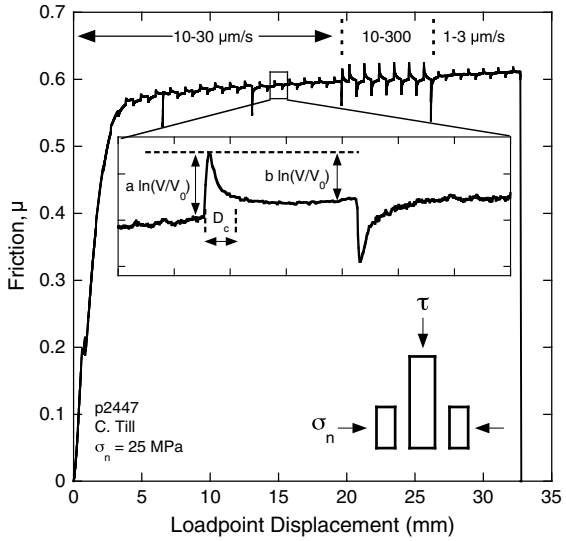

Figure 3. Friction-displacement curve for an entire experiment. The lower inset shows double direct shear arrangement. The main inset is a zoom of velocity step tests. Shearing velocity was stepped between values indicated on the top of the figure. Velocity steps begin at the initiation of shear, with each step lasting 450 µm.

Table 1. Experiment Data[a]

Experiment	Material	Layer Thickness (µm)	Normal Stress (MPa)
p1345	Caesar till	10	1
p1507	Caesar till	10	1
p1968	Medium sand	10	1
p1969	Medium sand	10	1
p1970	Fine-grained quartz	10	1
p2064	Medium sand	10	1
p2065	Medium sand	3	1
p2410	Medium sand	10	25
p2411	Medium sand	10	25
p2412	Medium sand	10	1
p2413	Fine-grained quartz	10	25
p2414	Medium sand	10	1
p2415	Medium sand	10	25
p2416	Medium sand	10	1
p2443	Fine-grained quartz	10	1
p2444	Fine-grained quartz	10	1
p2445	Medium sand	10	1
p2447	Caesar till	10	25
p2636	Medium sand	10	25–35 8 cycles
p2637	Medium sand	10	35
p2638	Granite blocks	0	5
p2645	Medium sand	7	25
p2646	Granite blocks	0	5
p2647	Medium sand	3	25
p2648	Medium sand	10	25–15 64 cycles
p2649	Medium sand	10	25
p2650	Medium sand	10	25

[a]Complete grain size distributions are presented in Figure 2. In experiments p2636 and p2648 the normal stress is cycled between the indicated values 8 and 64 times, respectively.

be found in the work of *Mair and Marone* [1999], *Karner and Marone* [2001], *Frye and Marone* [2002], and *Rathbun et al*. [2008]. Normal stress ranged from 1 to 40 MPa and was kept constant during shear. In all experiments, the nominal contact area was constant at 10 cm × 10 cm. The initial macroscopic shear zone thickness ranged from 1 cm in granular samples to 0 for bare surface experiments. Shearing velocity at the gouge layer boundaries was varied in a series of step changes ranging from 1 to 300 µm/s. This velocity range represents quasi-static conditions during the initiation of shear in a fault zone. Experiments were conducted in the absence of inertial effects and long-term weakening associated with high-speed friction experiments (more than tens of centimeters per second) that aim to represent slip during an earthquake. Instead, we concentrated on low velocity to study the possibility of acceleration of the fault to seismic slip rates. Complete normal stress, layer thickness, and shear velocity history for each experiment are presented in Table 1.

3. Results

3.1. Velocity Stepping Experiments

[17] Velocity step tests began at the initiation of shear and continued throughout the experiment (Figure 3). For granular layers, interparticle shear begins almost immediately upon application of shear load. Initially, the frictional strength increases rapidly and then levels off and becomes steady (Figure 3). For analysis of RSF parameters, we only consider velocity steps after friction has reached steady state, which occurs at a load-point displacement of ~5 mm (Figure 3). Velocity steps result in an immediate change in friction, with

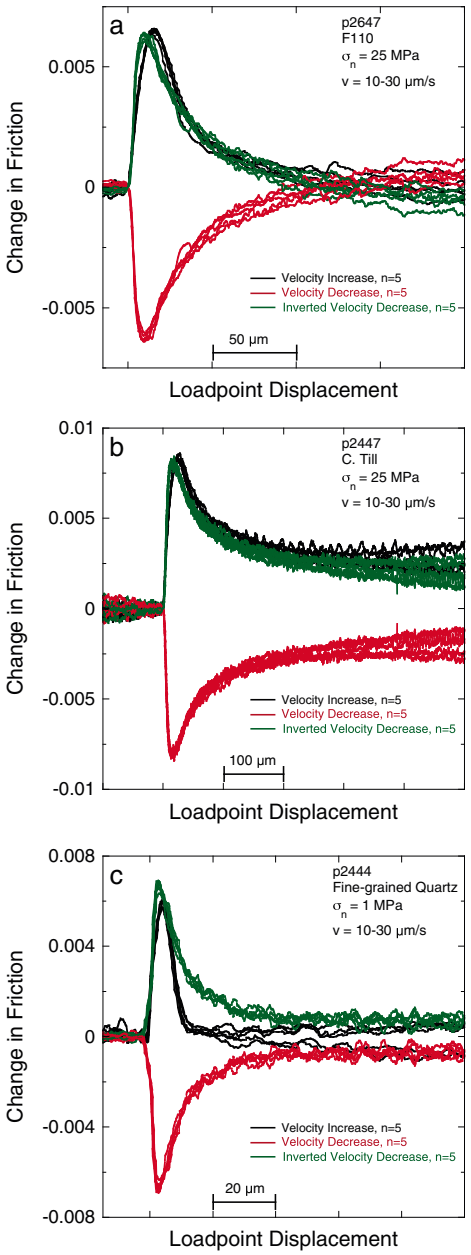

Figure 4. Velocity increases (black), decreases (red), and mirrored decreases (green) for (a) medium sand, (b) Caesar till, and (c) fine-grained quartz. For each panel, *n* indicates the number of steps shown. In all cases, velocity steps were between 10 and 30 μm/s, with medium sand and Caesar till at 25 MPa normal stress and fine-grained quartz at 1 MPa. All steps are consecutive and offset to facilitate comparison. Friction is plotted as the change from steady state sliding friction prior to the velocity step.

velocity increases (decreases) leading to pronounced peaks (drops) in friction followed by evolution back to steady state sliding friction (Figure 3, inset). The difference between friction before the step and the peak is referred to as the friction direct effect and is described by the RSF friction parameter *a*. The evolution of friction after the direct effect is described by the RSF parameters *b* and D_c, via the state evolution equation. The critical slip distance D_c is the *e*-folding slip distance from peak to steady state (Figure 3, inset). Due to the finite stiffness of the loading apparatus, the RSF parameters cannot be measured directly from a velocity step but must be obtained via modeling, accounting for the elastic loading stiffness (e.g., equation (4) and Figure 1).

[18] To assess the symmetry of frictional response, we compare a series of velocity increases and decreases of different magnitudes. Figure 4 presents 10 consecutive velocity steps (5 increases and 5 decreases) from experiments conducted on each granular material. Each step is plotted by lining up the point at which the velocity step occurs for easy comparison, with the velocity increases shown in black and decreases in red. The velocity decreases are inverted and shown as mirror images in green, e.g., Figure 1. Each velocity increase (decrease) shows remarkable reproducibility during the friction direct effect, when shear load increases (decreases) to a maximum (minimum). Our data are similar to the numerical steps presented in Figure 1: the velocity decreases have a higher apparent stiffness, as expected, as well as a smaller peak friction value. The measured *k* in our experiments was 0.001–0.002 μm^{-1}, corresponding to the intermediate case of *k* in Figure 1. The value of *k* is measured for each velocity step by fitting the initial linear elastic loading portion of the friction-displacement curve after a step change in velocity.

[19] Figure 4a presents velocity steps for medium sand. Comparison of the velocity increases to the inverted decreases shows that frictional evolution is initially different for the two cases but begins to match after a slip of ~25 μm, well before steady state friction is reached. Velocity steps for medium sand are near velocity neutral with some steps slightly velocity strengthening and some slightly weakening.

[20] Caesar till (Figure 4b) displays behavior similar to medium sand but with larger values for *a* and D_c. Velocity decreases and increases come to steady state at similar displacements, consistent with predictions of Ruina's law and not as expected for Dieterich's law. In all cases, velocity steps on till are velocity strengthening, consistent with previous results [*Rathbun et al.*, 2008; *Rathbun and Marone*, 2010]. Velocity steps on fine-grained quartz (Figure 4c) again show reproducibility for velocity increases and decreases. Due to velocity weakening and stick-slip behavior at high normal stress, data for fine-grained quartz are only presented at 1 MPa normal stress. In experiments on the fine-grained quartz, velocity increases reach steady state friction after ~10 μm of slip while velocity decreases reach steady sliding friction at ~25 μm, contrary to the predictions of both Ruina's law and Dieterich's law.

[21] For the three granular materials presented in Figure 4, the length of D_c for steady sliding friction correlates with the average grain size, consistent with previous work [*Dieterich*, 1981; *Sammis and Biegel*, 1989; *Marone and Kilgore*, 1993]. For the finest grained material, fine-grained quartz, steady friction is established by ~10 μm for velocity increases and ~25 μm for decreases. Increasing the average grain size to that of medium sand lengthens the distance to steady sliding friction to ~100 μm for both velocity increases and decreases. In the case of our largest grains, glacial till, steady friction is not established until the displacement is >200 μm.

[22] Increasing the size of the velocity perturbation by an order of magnitude to 10–300 μm/s increases the size of the friction peak for both velocity increases and decreases and lengthens the displacement needed to reach

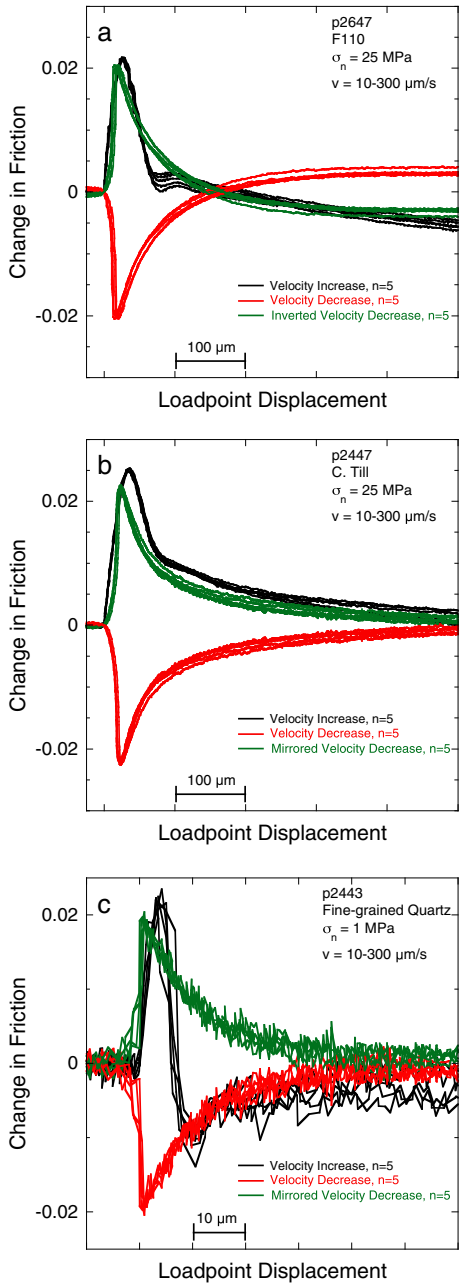

Figure 5. Velocity increases (black), decreases (red), and mirrored decreases (green) between 10 and 300 μm/s for (a) medium sand, (b) Caesar till, and (c) fine-grained quartz for 10 consecutive steps. Note the asymmetric behavior for velocity increases and decreases, particularly for the quartz.

a new steady friction level (Figure 5a). Again, each step is nearly indistinguishable for velocity decreases; however, the increases show separate minima ~75 μm after the velocity step. This minimum in the friction is only observed for the velocity increases and represents an elastic effect from the rapid change in stress of the apparatus. The decreases show a smooth evolution to steady state, the same as in the smaller steps.

[23] Till also displays differences in behavior between increases and decreases for large steps (Figure 5b). Velocity decreases show a smooth transition to steady state while increases display a break in the trend similar to that illustrated in Figure 5a, albeit at a larger displacement. In both Figures 5a and 5b, the first length scale associated with friction evolution for velocity increases is smaller than that for velocity decreases. The second length scale increases the total displacement required to establish steady friction. As a result of the second length scale, velocity increases and decreases reach steady state at approximately the same displacement, but with different shapes. Experiments on fine-grained quartz and the smallest D_c show a clear difference in length scales for increases and decreases (Figure 5c). Velocity increases evolve to steady state over ~10 μm, while velocity decreases require a much longer displacement. As with medium sand, an elastic effect and minima are observed during the velocity increases, but the difference in increases and decreases is pronounced.

3.2. Dilation and Compaction During Velocity Steps

[24] Each perturbation in velocity causes an associated change in layer thickness. Velocity increases result in layer dilation and velocity decreases result in compaction (e.g., Figure 6). Previous investigators have used the amount of dilation as a proxy for localization in a shearing layer [e.g., *Marone and Kilgore*, 1993; *Saffer and Marone*, 2003; *Rathbun and Marone*, 2010]. We expand on these works, comparing the relative amounts of dilation and compaction for the velocity steps in our experiments. Following standard procedure [i.e., *Scott et al.*, 1994], we remove a linear trend of decreasing layer thickness with slip, which results from geometric thinning of the layer with shear. Layer thickness change is presented for 10 consecutive steps in Figure 6. As with plots of friction evolution, each step is offset for comparison.

[25] Figure 6a presents the change in layer thickness for representative steps on medium sand at 25 MPa with velocity steps between 10 and 30 μm/s. Dilation is given as a positive change in layer thickness and compaction as a negative change. As with the friction curves (Figures 4 and 5), the compaction associated with velocity decreases is mirrored for comparison to velocity increases. After a velocity increase, the layer dilates ~1 μm for an initially 10 mm thick sample, while after a decrease, the layer compacts ~1.5 μm (Figure 6a). As with the friction curves, layer thickness trends are reproducible with good agreement of five consecutive increases and decreases. Experiments on Caesar till have the largest values for dilation/compaction and more variability between each step (Figure 6b). As with medium sand, the largest values of layer thickness change are associated with velocity decreases, but the two populations show overlap in layer thickness change. Experiments on fine-grained quartz display the largest disparity between velocity increases and decreases (Figure 6c), with a clear separation between increases and decreases. Decreases in velocity compact the layer ~2 times as much as increases dilate the layer. Measurements of layer dilation and compaction have been verified using independent measurements of fluid volume change during dilation and compaction [e.g., *Samuelson et al.*, 2009].

[26] The change in layer thickness and the difference between compaction and dilation scale with grain size in our experiments [e.g., *Samuelson et al.*, 2011]. The largest grain size, till, has the largest dilation/compaction, followed

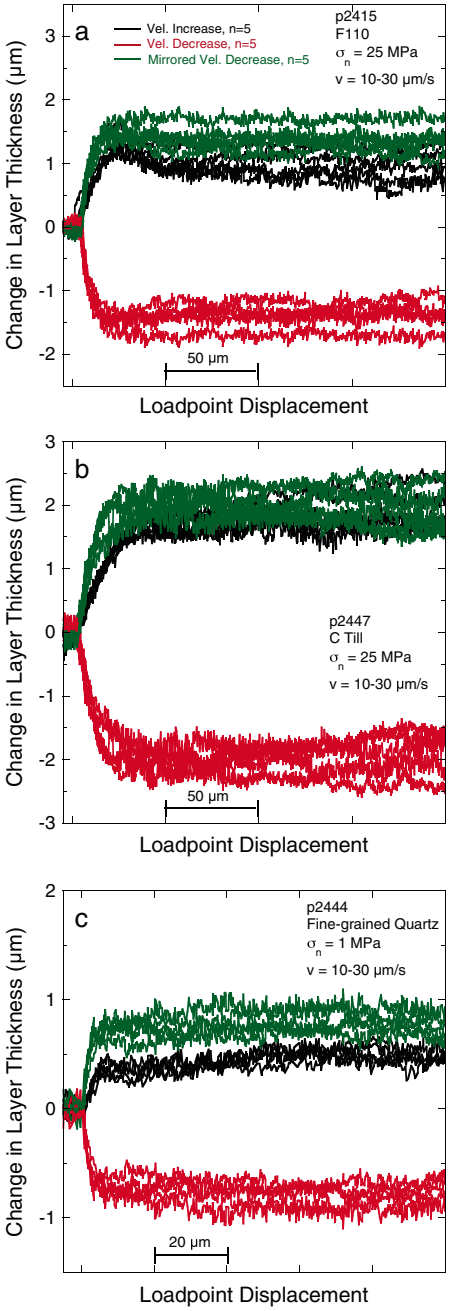

Figure 6. Change in layer thickness for velocity increases (black) and decreases (red), with the decreases mirrored (green). Upon a velocity increase the layer dilates, and upon a decrease the layer compacts. Each panel shows 10 consecutive velocity steps, 5 increases and 5 decreases, between 10 and 30 μm. (a) Medium sand at 25 MPa normal stress. (b) Caesar till at 25 MPa. (c) Fine-grained quartz at 1 MPa. Note that changes in layer thickness are similar for increases and decreases but that the magnitude of the change is larger for decreases.

by medium sand and then fine-grained quartz (Figure 6). The separation between the dilation and compaction in till is unclear for steps between 10 and 30 μm/s; however, it appears that compaction is slightly larger than dilation (Figure 4b). In medium sand, compaction is generally larger than dilation, with some overlap between the two, while in fine-grained quartz, there is a clear separation between dilation and compaction.

[27] Increasing the size of the velocity steps to 10 to 300 μm/s highlights the difference between increases and

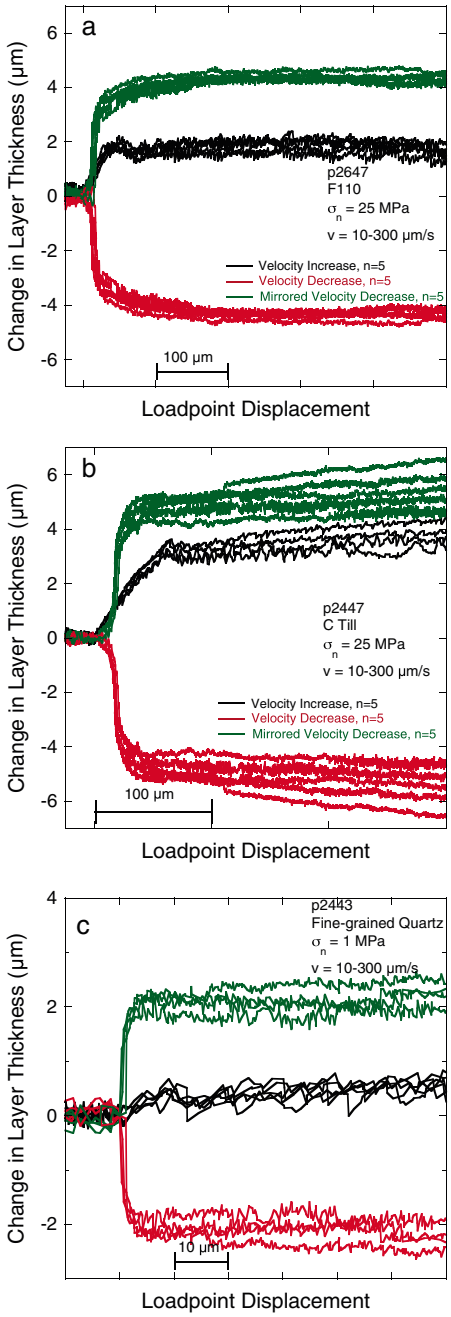

Figure 7. Change in layer thickness for velocity increases (black) and decreases (red), with the decreases mirrored (green), for velocity steps between 10 and 300 μm/s. The layer thickness data correspond to the friction data shown in Figure 5. Each panel shows 10 consecutive velocity steps, 5 increases and 5 decreases, between 10 and 30 μm. (a) Medium sand at 25 MPa normal stress. (b) Caesar till at 25 MPa. (c) Fine-grained quartz at 1 MPa. Note that compaction during velocity decreases is larger in magnitude than dilation during velocity increases.

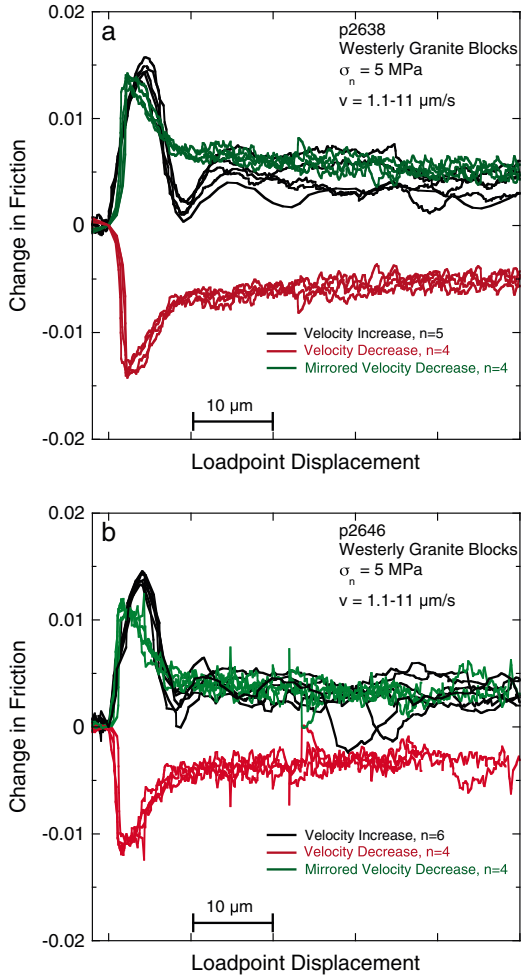

Figure 8. Comparison of 10X velocity increases (black) and decreases (red), with the decreases mirrored (green), for two experiments on bare Westerly granite surfaces. Normal stress was 5 MPa in both experiments. In both panels, *n* corresponds to the number of velocity steps. Note that velocity increases have a larger direct effect followed by a drop in friction that is not mimicked in velocity decreases.

decreases (Figure 7). Factor of 30 velocity increases and decreases on medium sand show ~2 times more compaction than dilation after a 3X velocity step (Figure 7). The compaction increases from ~1.5 μm on small steps to 4 μm on large steps, while the dilation increases from 1 to ~2 μm for small and large steps, respectively. Comparing the increases versus decreases in the large steps indicates that the rate of change of layer thickness is larger for velocity decreases. As with the dilation/compaction for small velocity steps, till displays less disparity than medium sand between velocity increases and decreases (Figures 7a and 7b), with greater changes in layer thickness in the larger grain-sized till. In fine-grained quartz, the dilation after a velocity increase is 0.5 μm or less and the compaction is ~2 μm (Figure 7c). In all cases, the compaction is larger than the dilation.

3.3. Bare Surface Experiments

[28] Two experiments on roughened bare granite surfaces show that D_c is the same for velocity increases and decreases (Figure 8). Both bare surface experiments show more variability than experiments on granular materials but still yield reproducible results both between and within individual experiments. Velocity increases show an elastic response due to overshoot and a pronounced drop in friction at ~8 μm of displacement (Figure 8a), but the displacement needed to attain steady state is the same for increases and decreases. Steps from experiment p2646 (Figure 8b) slide stably at 11 μm/s. This difference is likely caused by subtle differences in surface roughness between the samples.

[29] The frictional response for bare granite surfaces (Figure 8b) is consistent with the RSF theory (Figure 1), which predicts that decreases in velocity reach a friction minimum at a smaller displacement than velocity increases. Also, the friction minimum (direct effect) is smaller in magnitude for velocity decreases than for increases. The evolution to steady state then occurs with both increases and decreases reaching steady sliding friction at ~8 μm (Figure 8). As with the experiments on granular materials, the velocity decreases do not evolve to steady friction at smaller displacements, as predicted by Dieterich's law. The displacement needed to reach steady state is the same for all cases in our bare surface experiments, which is most consistent with Ruina's law (Figure 1b).

3.4. Normal Stress Oscillations

[30] To evaluate the effects of shear localization and granular packing on RSF behavior, we conducted a series of experiments in which normal stress was oscillated midway

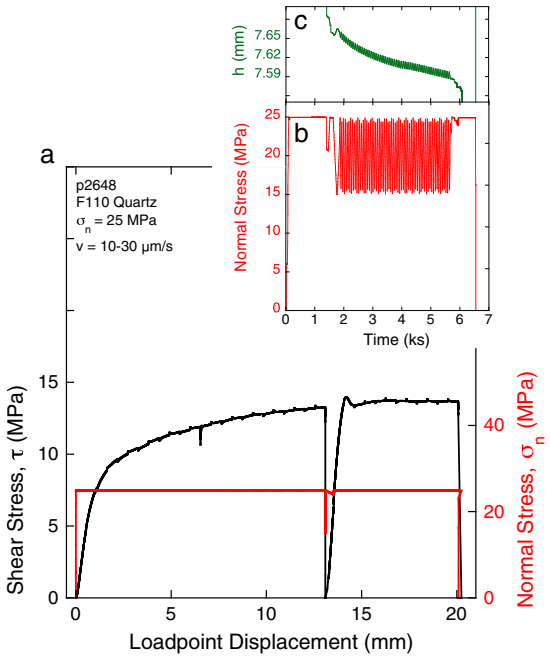

Figure 9. Main plot shows data for a complete experiment, friction (black), and normal stress (red) versus displacement. Velocity step tests are conducted between 10 and 30 μm/s. At ~13 mm, shear stress was removed and (upper panel) normal stress was oscillated between 25 and 15 MPa with a period of 60 s for 64 cycles. The uppermost panel shows layer thickness change, compaction, during the stress oscillations. Shear resumed at constant normal stress after the normal stress oscillations.

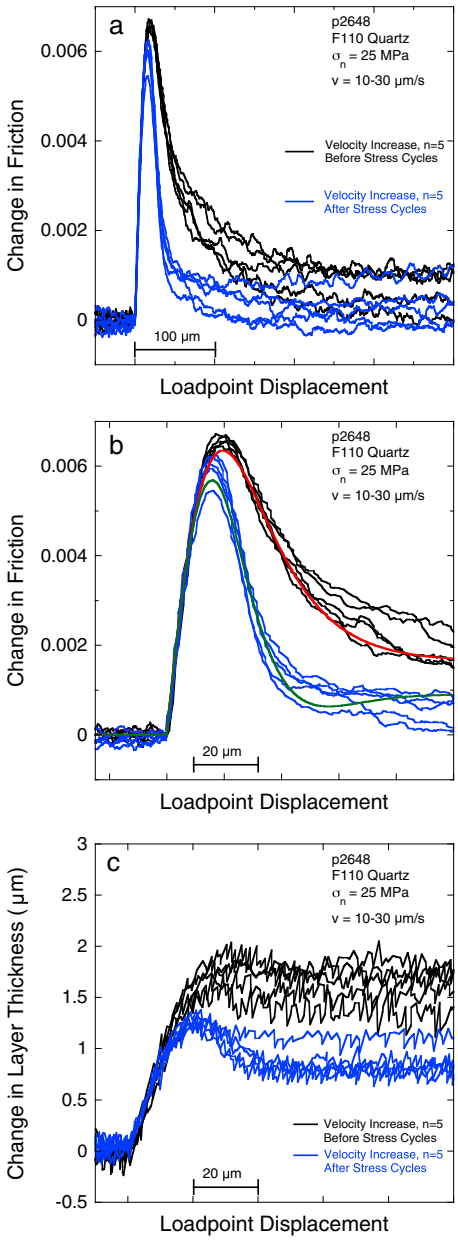

Figure 10. Velocity steps from 10 to 30 μm/s before and after normal stress oscillations (see Figure 9). (a) Five steps immediately preceding (thin black lines) and following (thin blue) the oscillations. Oscillations work to decrease the peak friction and the slip required to reach a new steady sliding friction. (b) The friction data from Figure 10a along with RSF simulations. The red line, with pre-oscillation data, shows $a = 0.0073$, $b = 0.0063$, and $D_c = 36$ μm. The green line, with post-oscillation data, shows $a = 0.0075$, $b = 0.007$, and $D_c = 16$ μm. (c) Corresponding changes in layer thickness for velocity steps are presented in Figures 10a and 10b. Note that layer thickness changes are larger prior, compared to after, the normal stress oscillations.

through the run, following the procedures of *Richardson and Marone* [1999] and *Boettcher and Marone* [2004]. In these experiments, shear was imposed using our normal procedure for ~13 mm (Figure 9), after which shear stress was removed and normal stress was oscillated between 15 and 25 MPa at a period of 1 min for 64 min. Layer compaction occurred during the normal stress oscillations (Figure 9c). For the run shown in Figure 9, the layer compacted from ~7.65 to ~7.59 mm, corresponding to a porosity loss of 0.8 porosity units (Figure 9b). In another experiment of this series, normal stress was increased in a series of eight cycles between 25 and 35 MPa, at a period of 15 min, which produced layer compaction of 30 μm or 0.4 porosity units.

[31] We compare RSF behavior in velocity steps before and after the normal stress oscillations (Figure 10). The oscillations reduce both the direct effect peak friction and the distance required to evolve back to steady state. Figure 10b presents forward models overlying the two sets of velocity steps. The RSF parameters are $a = 0.0073$, $b = 0.00625$, and $D_c = 36$ μm before oscillations and $a = 0.0075$, $b = 0.007$, and $D_c = 16$ μm after oscillations using Ruina's law. We choose to only use one state variable in the models, even though there is considerable misfit (Figure 9b).

[32] The friction direct effect and peak friction are smaller after the stress oscillations and the magnitude of layer dilation is also smaller. For the same 3X velocity increase, the layer dilated ~1.5 μm prior to normal stress oscillations compared to ~0.75 μm after the oscillations (Figure 9c). This difference can be interpreted as a decrease in the thickness of the active shear zone after the normal stress oscillations, localizing the shear zone and solidifying the spectator regions of the layer via tighter granular packing and reduced porosity. It is interesting to note that the reduction of D_c associated with dynamic stressing suggests a possible mechanism for dynamic earthquake triggering. That is, if the passage of seismic waves has an effect on fault zone friction similar to that in Figure 10, the associated change in the critical stiffness could lead to instability. Our data show that dynamic stressing reduces both D_c and the friction rate parameter ($b - a$); thus, the change in K_c (see equation (5) below) is somewhat smaller than if ($b - a$) were unchanged. Although this topic is beyond the scope of the present study, it is clearly worthy of additional study.

4. Discussion

4.1. Which Law?

[33] We find that Ruina's law, which predicts that velocity increases and decreases should reach steady state at equal displacements, best matches our experimental data, although we find important departure from predictions of Ruina's law. Dieterich's law predicts that velocity decreases should reach steady sliding friction at a smaller displacement than increases due to the importance of contact time. Our results for 3X velocity steps indicate that velocity increases and decreases reach steady state at similar displacements or, in some cases, velocity increases reach steady state at smaller displacements than decreases (Figure 4). Increasing the size of the velocity steps, to 10X or 30X, causes a change in behavior, with velocity increases showing two-state behavior while velocity decreases still only exhibit one length scale in the return to steady state (Figure 5). The first length scale for the 30X velocity steps is smaller for velocity increases than for decreases. However, the second length scale is larger for velocity increases, consistent with Dieterich's law, and thus the total evolution distance of friction is similar in both cases. In

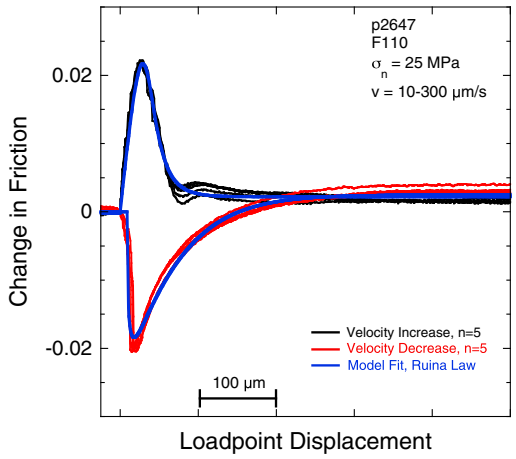

Figure 11. Friction data for five velocity increases and decreases along with best fit RSF models using Ruina's law. The parameters for velocity increases are $a = 0.0079$, $b = 0.0072$, and $D_c = 31.2$ μm; those for velocity decreases are $a = 0.0070$, $b = 0.0077$, and $D_c = 59.8$ μm.

cases where one length scale controls frictional instability and/or state evolution, velocity increases clearly reach steady state at a lower displacement than decreases (Figure 5c).

[34] Figure 11 presents the best fit RSF models for 30-fold velocity steps on medium sand with Ruina's law. Models match the evolution of velocity decreases with $a = 0.0070$, $b = 0.0077$, and $D_c = 59.8$ μm. For velocity increases, models fit the direct effect and evolution in friction but do not capture the local minimum at ~80 μm after the velocity step. The best fit model for five velocity increases is $a = 0.0079$, $b = 0.0072$, and $D_c = 31.2$ μm when ignoring the minimum and following long-term evolution. The initial peak and evolution of friction for the velocity increases are smaller than those for the decreases, but the long-term evolution extends D_c.

[35] These data support the hypothesis of *Rathbun and Marone* [2010], who showed that for experiments on glacial till at 1 MPa normal stress, a longer critical slip distance was required to fit their data with velocity decreases when using Dieterich's law. This led to the assertion that Ruina's law best described their experiments. Our result contrasts with the results of the slide-hold-slide healing experiments of *Beeler et al*. [1996], who showed that Dieterich's law best matched their data. We observe behavior consistent with neither Ruina's law nor Dieterich's law in that velocity increases can evolve to steady sliding friction at a smaller displacement than velocity decreases (i.e., Figures 4c and 5c).

[36] Our results indicate that neither of the commonly used state evolution laws is adequate to describe the full range of laboratory data. As noted above, previous research has reached a similar conclusion. The composite law proposed by *Kato and Tullis* [2001] to explain the experiments of *Beeler et al*. [1994] emphasizes time-dependent aging. Typically, the RSF laws have not included chemical [e.g., *Bos et al*., 2000; *Frye and Marone*, 2002; *Niemeijer and Spiers*, 2007; *Niemeijer et al*., 2008] or thermal [*Chester and Higgs*, 1992; *Blanpied et al*., 1995, 1998; *Chester*, 1994; *Den Hartog et al*., 2012a, 2012b] effects explicitly, although these are well documented. In our study, we only attempt to evaluate the two most commonly used laws that form the basis for most models of earthquake rupture [e.g., *Heaton*, 1990; *Beeler and Tullis*, 1996; *Ampuero et al*., 2002; *Lapusta and Rice*, 2003; *Ziv and Rubin*, 2003]. A rigorous test of other alternative forms of the laws is beyond the scope of this study. However, we note that none of the alternative forms of the state evolution laws considers a changing shear zone thickness, which is an important feature of our data.

[37] *Sleep* [2005] attempted to provide a physical basis for the two common laws concentrating on healing when $V = 0$, rather than sliding. *Sleep* [2005] argued that Ruina's law arises from exponential creep at contacts and scales with contact size, while Dieterich's law arises from creep for both shear and compaction at the subgranular scale. He also attempted to place bounds on the applicability of each law with the slip law occurring at low humidity and the aging law at high humidity [i.e., *Frye and Marone*, 2002]. We find that the slip law better approximates our data in experiments conducted at room temperature and humidity.

4.2. The Role of Shear Fabric in Asymmetry of Granular RSF Friction

[38] We propose that asymmetry in the frictional response for velocity increases and decreases is caused by changes in the shear fabric within granular layers. In our standard suites of experiments and in the experiments with normal stress oscillations, we posit that grain-to-grain interactions and interplay between the localized shear zone and surrounding spectator regions exert a strong influence on RSF behavior. One evidence for this hypothesis is the inequality in the magnitude of dilation for velocity increases versus compaction upon decreases (Figure 7).

[39] In a granular layer, dilation is driven by shear stress and local grain rearrangement [*Reynolds*, 1885; *Mead*, 1925]. In our experiments, dilation initially occurs throughout the layer as shear stress increases and then shear localization occurs when frictional strength reaches steady state [*Rathbun and Marone*, 2010]. With additional shear localization, a shear fabric develops and the magnitude of layer dilation is reduced. Thus, during a velocity step test in which velocity is increased, dilation is expected to be proportional to the width of the active shear zone and independent of spectator regions within which grain rearrangement is negligible. On the other hand, for a decrease in velocity, the drop in shear stress is felt throughout the layer and thus compaction is expected to occur throughout the layer. This fundamental asymmetry arises because granular dilation requires shear strain and interparticle slip, whereas compaction can occur simply as a result of a change in stress.

[40] In the case of a localized shear zone, we expect that dilation will be smaller than compaction because only the localized zone can dilate, whereas the entire layer can compact. For the 3X velocity steps, the layer compacts slightly more than it dilates after a velocity step (Figure 6). When the step size is increased to 30X, the difference between dilation and compaction is greater (Figure 7). The difference between dilation and compaction suggests differences in the micromechanics of the layer during each of the directional changes in velocity. These data are consistent with the hypothesis that during dilation only the active shear band dilates as a result of the velocity change.

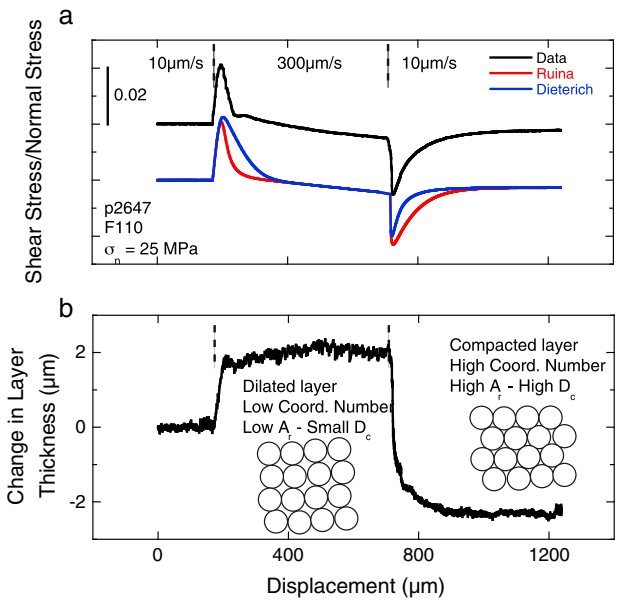

Figure 12. (a) Friction data for two velocity steps with medium sand. The red line shows the best fit RSF model with Ruina's law (parameters given in Figure 11). The blue line shows Dieterich's law for these same parameters. (b) Layer thickness change for the velocity steps in Figure 12a. After an increase in velocity, the layer dilates, leading to low coordination numbers and a smaller real contact area; after a decrease in velocity, the layer compacts, increasing the contact area. The schematic inset shows the hypothesized changes in the actively shearing layer. A velocity increase dilates the layer, decreasing the real contact area.

[41] In granular materials, shear localizes into discrete zones that are typically several to ~20 particles thick [e.g., *Muhlhaus and Vardoulakis*, 1987; *Tordesillas et al*., 2004; *Rathbun and Marone*, 2010; *Rathbun et al*., 2013], with grain size distribution controlling the thickness of the localized zone in compaction studies [*Cheung et al*., 2012]. *Marone and Kilgore* [1993] proposed a model in which the critical slip distance for friction derives from shear bandwidth and granular particle dimension. We propose a variant of that model in which changes in the active shear zone width combine with state evolution of particle contact junctions to produce friction evolution and the observed critical slip distance.

[42] We find that during a velocity increase the layer initially dilates (Figure 12a). This dilation causes a slight decrease in the contact area, A_r, between particles in the granular shear zone due to changes in porosity and granular packing. After dilation, the average number of contacts of each grain (coordination number) decreases, changing A_r (e.g., Figure 12a). We expect that individual particle contact junctions are velocity weakening [*Marone et al*., 1990], which would promote further granular shear localization.

[43] These ideas support a model in which dilatancy and changes in A_r tend to further localize shear, leading to smaller values of D_c for velocity increases. On the other hand, for a velocity decrease, the layer compacts, which increases A_r and the coordination number for contact junctions within the active shear zone, leading to grain strengthening and interlocking, both of which will tend to broaden the zone of active shear. Because the shear zone involves more contacts, D_c is larger for step decreases in the sliding velocity (Figure 12b).

[44] This model of RSF in granular systems is supported by our experiments with normal stress oscillations. Normal stress oscillations reduced porosity and compacted layers (Figure 9). After the oscillations, velocity step tests showed significant differences compared to prior values (Figure 10). We found that the friction direct effect was smaller and that D_c and layer dilation upon a step increase in velocity decreased by approximately a factor of 2 after normal stress oscillations.

[45] The decrease in both D_c and a is consistent with a narrower shear zone after the stress oscillations. A thicker active shear zone and more distributed deformation cause a larger a because more interparticle contact junctions need to be broken after the velocity perturbation. The evolution of D_c also points to an increase in the degree of localization after the stress oscillations. *Marone and Kilgore* [1993] showed that D_c scales with granular shear zone thickness. Our experiments support this interpretation (Figure 13). For all three granular materials, we find that D_c scales with layer dilation, Δh, and that larger velocity changes yield larger values of D_c and Δh.

[46] Our comparison of results for velocity increases and decreases, along with the normal stress oscillation experiments, points to a model in which shear zone thickness varies with slip rate and frictional state. We envision that the localized zone of active shear expands and shrinks by incorporating particles from the surrounding transitional and spectator regions (Figure 14). During the compaction resulting from a decrease in shear velocity and locking of the localized shear zone, the central portion of that zone strengthens, which causes slip between particles in the surrounding region. The transitional zone between the spectator

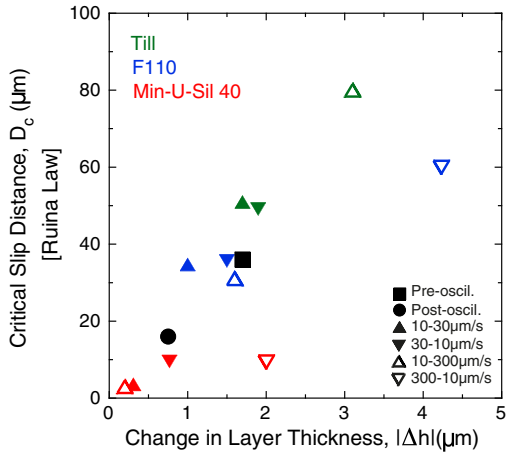

Figure 13. Critical slip distance and the change in layer thickness for velocity stepping experiments. Change in layer thickness is given as the absolute value of the change. Symbol color shows the material type, with closed symbols representing steps between 10 and 30 μm/s and open symbols between 10 and 300 μm/s. The point of the triangle represents velocity increases or decreases. Solid squares and circles represent normal stress oscillation experiments. The value of D_c is determined from models using Ruina's law.

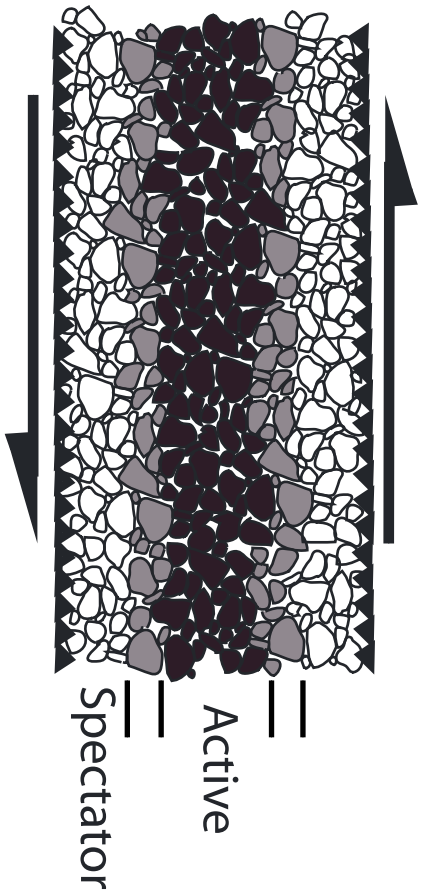

Figure 14. Schematic shear zone showing an actively shearing region (black), a spectator zone (white), and a transitional zone (grey). For a step decrease in slip velocity, compaction occurs in all zones. For a step increase in slip velocity, dilation occurs primarily in the zone of active shear, with some dilation in the transitional zone. Grains in the spectator zone do not undergo local relative motion and thus dilation is negligible in that region. We posit that the active shear zone expands into the transitional zone during velocity increases but not during velocity decreases.

region and the zone of active shear involves particles that alternate between active and passive states due to RSF effects at the particle scale, at contact junctions, and granular effects. The incorporation of more material into the active shearing zone causes increased values of both D_c and Δh, as shown in Figure 13.

[47] The frictional response to velocity increases and decreases is asymmetric for all three of the granular materials we studied. This asymmetry is not predicted by either Ruina's law, which predicts symmetry, or Dieterich's law, which predicts asymmetry opposite to that of our experiments.

4.3. Two-State Frictional Behavior

[48] Our velocity stepping experiments show two-state frictional behavior in some cases. We suggest that granular dilatancy dictates one length scale and that interparticle contact junctions dictate the other. Two-state variable behavior is particularly apparent in our largest magnitude velocity (Figure 5). Velocity increases have a pronounced and sharp frictional peak that decays toward a steady state and then incorporates another length scale for both medium-sand quartz and till. Two-state behavior has been noted in previous work [e.g., *Blanpied and Tullis*, 1986; *Cox*, 1990; *Marone et al*., 1990; *Marone and Cox*, 1994; *Blanpied et al*., 1998]. *Cox* [1990] argued that two-state behavior was caused by a longer D_c related to the structure in the gouge zone, while the shorter D_c was related to the evolution of surface properties. *Marone and Cox* [1994] conducted experiments on bare surfaces of gabbro with varying surface roughness. They found that the second D_c disappeared with increasing displacement. This led *Marone and Cox* [1994] to conclude that their D_{c2} was a surface effect and that D_{c1} was a property of the gouge. They concluded that D_c in granular experiments could be thought of as the accumulation of several D_c values from grain-to-grain interactions [i.e., *Marone and Kilgore*, 1993].

[49] In our experiments, we observed a difference in the compaction/dilation of the layer associated with velocity steps, which we argue is the result of localization. Caesar till has been shown to localize shear into a finite boundary-parallel zone [*Rathbun and Marone*, 2010], whereas medium-sand quartz is well known to localize shear onto Y and R shears. We infer that the two-state behavior observed is the result of changes in the micromechanics of the localized shear zone. During velocity increases, the first length scale is associated with grain-to-grain contacts and frictional evolution and the second with a length to dilate the localized shear zone. It seems likely that a length scale to dilate the layer is present in steps of all sizes; however, that D_c is only observed when the step size increases to a large enough magnitude.

4.4. Implications for the Stability of Fault Zones

[50] Changes in shear zone thickness and frictional behavior during shear have implications for the stability of faults and earthquake triggering by dynamic stresses. The model of *Bizzarri* [2010] considers the width of a fault zone during shear. Wear is produced during shear, with the entire gouge zone assumed to be contributing to shear. As the fault gouge zone increases in width, the recurrence time between slip events decreases and the temperature evolution and amounts of coseismic slip are changed.

[51] The stability of frictional sliding can be described in terms of a critical stiffness. Sliding is unstable when the loading stiffness is smaller than a critical value given by the RSF parameters [*Rice and Ruina*, 1983]:

$$k < k_c = \frac{-(a-b)\sigma_n}{D_c}\left[1 + \frac{mV^2}{\sigma_n a D_c}\right] \tag{5}$$

where a, b, and D_c are the RSF parameters; m is the mass per unit area; and V is velocity. During nucleation of unstable slip, when V is very low, the second term is negligible in comparison to the first, yielding:

$$k < k_c = \frac{-(a-b)\sigma_n}{D_c}. \tag{6}$$

[52] In this formulation, the RSF parameters a, b, and D_c and the normal stress, σ_n, define a critical stiffness, k_c. When k_c exceeds the stiffness of the laboratory apparatus and sample or the stiffness of the crustal rocks in natural systems, conditions are sufficient for earthquakes to occur.

[53] In our experiments with normal stress oscillations, both a and D_c decrease after the vibrations, leading to a greater potential for unstable frictional slip. It is a necessary but insufficient condition that the $(a - b)$ term in equation (5) is negative, the velocity weakening condition, for an earthquake to occur. A decrease in the peak friction, as shown in Figure 10, yields a smaller term for $(a - b)$ and could cause a transition from stable creep to dynamic earthquake rupture, as envisaged in models of earthquake triggering [e.g., *Parsons*, 2005, *Johnson et al*., 2012]. *Faulkner et al*. [2011] conducted low stress experiments and suggested that earthquake propagation is dominated by parameters other than only $(a - b)$. At high slip velocities, samples weaken at small critical slip distances, resulting in low fracture energy for nucleation of slip [*Faulkner et al*., 2011]. It is possible that the consolidation events we documented in association with dynamic stresses, which cause reduced D_c and/or friction parameter a, may be a mechanism for earthquake triggering.

5. Conclusions

[54] For velocity stepping experiments on granular materials, Ruina's law better describes our results than Dieterich's law. We demonstrate that an asymmetry between velocity increases and decreases occurs in velocity-strengthening glacial till, velocity-weakening fine-grained quartz, and medium sand-sized quartz, which transitions from strengthening to weakening. Experiments on bare surfaces of Westerly granite blocks produce a symmetric or near-symmetric response for velocity increases and decreases. The asymmetry we observed is not predicted by either of the commonly used evolution laws. We propose a new conceptual model based on micromechanics of granular shear and changes in the thickness of the actively shearing zone to explain asymmetry. Experiments using normal stress oscillation and velocity step tests show that both the critical slip distance and the friction direct effect decrease as a result of layer compaction, which supports a model in which shear localization in an active zone dictates the granular RSF response. Shear localization also works to produce two distinct length scales and two-state evolution behavior for frictional evolution. Localization produces a smaller critical slip distance, which enhances the likelihood of seismic slip and is a potential mechanism for dynamic triggering and shallow aftershocks.

[55] **Acknowledgments.** Grain size characterization was conducted at the Materials Characterization Lab (MCL) of Penn State University. This work benefited from comments by Bryan Kaproth on an early draft. We thank editor Tom Parsons and associate editor John Spray for their comments.This work was supported by NSF though awards EAR-0911569, OCE-0648331, EAR-0746192, and EAR-0950517.

References

Ampuero, J.-P., and A. M. Rubin (2008), Earthquake nucleation on rate-and-state faults: Aging and slip laws, *J. Geophys. Res.*, *113*, B01302, doi:10.1029/2007JB005082.

Ampuero, J.-P., J.-P. Vilotte, and F.-J. Sánches-Sesma (2002), Nucleation of rupture under slip dependent friction law: simple models of fault zone, *J. Geophys. Res.*, *107*(B12), 2324, doi:10.1029/2001JB000452.

Bayart, E., A. M. Rubin, and C. Marone (2006), Evolution of fault friction following large velocity jumps, *Eos. Trans. AGU*, *87*(52), Fall Meet. Suppl. Abstract S31A-0180.

Beeler, N. M. (2009), Constructing constitutive relationships for seismic and aseismic fault slip, *Pure Appl. Geophys.*, *166*, 1775–1798, doi:10.1007/s00024-009-0523-0.

Beeler, N. M., and T. E. Tullis (1996), Self-healing slip pulses in dynamic rupture models due to velocity dependent strength, *Bull. Seismol. Soc. Am.*, *86*, 1130–1148.

Beeler, N., T. Tullis, and J. Weeks (1994), The roles of time and displacement in the evolution effect in rock friction, *Geophys. Res. Lett.*, *21*, 1987–1990.

Beeler, N. M., T. E. Tullis, M. L. Blanpied, and J. D. Weeks (1996), Frictional behavior of large displacement experimental faults, *J. Geophys. Res.*, *101*(B4), 8697–8715.

Bizzarri, A. (2010), On the recurrence of earthquakes: Role of wear in brittle faulting, *Geophys. Res. Lett.*, *37*, L20315, doi:10.1029/2010GL045480.

Blanpied, M. L., and T. E. Tullis (1986), The stability and behavior of a frictional system with a two state variable constitutive law, *Pure Appl. Geophys.*, *124*, 415–430.

Blanpied, M. L., D. A. Lockner, and J. D. Byerlee (1995), Frictional slip of granite at hydrothermal conditions, *J. Geophys. Res.*, *100*(B7), 13,045–13,064.

Blanpied, M. L., C. Marone, D. A. Lockner, J. D. Byerlee, and D. P. King (1998), Quantitative measure of the variation in fault rheology due to fluid-rock interactions, *J. Geophys. Res.*, *103*, 9691–9712.

Boettcher, M. S., and C. Marone (2004), The effect of normal force vibrations on the strength and stability of steadily creeping faults, *J. Geophys. Res.*, *109*, B03406, doi:10.1029/2003JB002824.

Bos, B., C. J. Peach, and C. J. Spiers (2000), Slip behavior of simulated gouge-bearing faults under conditions favoring pressure solution, *J. Geophys. Res.*, *105*, 16,669–16,718.

Cashman, S. M., and K. V. Cashman (2000), Cataclasis and deformation-band formation in unconsolidated marine terrace sand, Humboldt County, California, *Geology*, *28*, 111–114.

Cashman, S. M., J. N. Baldwin, K. V. Casman, K. Swanson, and R. Crawford (2007), Microstructures developed by coseismic and aseismic faulting in near-surface sediments, San Andreas fault, California, *Geology*, *35*, 611–614.

Chester, F. M. (1994), Effects of temperature on friction: Constitutive equations and experiments with quartz gouge, *J. Geophys. Res.*, *99*, 7247–7261.

Chester, F. M., and J. S. Chester (1998), Ultracataclasite structure and friction processes of the Punchbowl fault, San Andreas system, California, *Tectonophysics*, *295*, 199–221.

Chester, F. M., and H. G. Higgs (1992), Multimechanism frictional constitutive model for ultrafine quartz gouge at hypocentral conditions, *J. Geophys. Res.*, *97*(B2), 1859–1870.

Cheung, C. S. N., P. Baud, and T. Wong (2012), Effect of grain size distribution on the development of compaction localization in porous sandstone, *Geophys. Res. Lett.*, *39*, L21302, doi:10.1029/2012GL053739.

Cox, S. J. D. (1990), Velocity dependent friction in a large direct shear experiment on gabbro, in *Deformation Mechanisms, Rheology, and Tectonics*, edited by R. J. Knipe and E. H. Rutter, Geol. Soc. London Spec. Publ., *54*, 63–70.

den Hartog, S. A. M., A. R. Niemeijer, and C. J. Spiers (2012a), New constraints on megathrust slip stability under subduction zone P-T conditions, *Earth Planet. Sci. Lett.*, *353–354*, 240–252, doi:10.1016/j.epsl.2012.08.022.

den Hartog, S. A. M., C. J. Peach, D. A. Matthijs de Winter, C. J. Spiers, and T. Shimamoto (2012b), Frictional properties of megathrust fault gouges at low sliding velocities: New data on the effects of normal stress and temperature, *J. Struct. Geol.*, *38*, 156–171, doi:10.1016/j.jsg.2011.12.001.

Dieterich, J. H. (1979), Modeling of rock friction: 1. Experimental results and constitutive equations, *J. Geophys. Res.*, *84*(B5), 2161–2168.

Dieterich, J. H. (1981), Constitutive properties of faults with simulated gouge, in *Mechanical Behavior of Crustal Rocks*, Geophys. Mono. Ser., vol. 23, edited by N. L. Carter, et al., pp. 103–120, AGU, Washington DC.

Dieterich, J. H., and B. Kilgore (1994), Direct observation of frictional contacts – new insights for state-dependent properties, *Pure Appl. Geophys.*, *143*, 283–302.

Faulkner, D. R., A. C. Lewis, and E. H. Rutter (2003), On the internal structure and mechanics of large strike-slip fault zones: field observations of the Carboneras fault in southeastern Spain, *Tectonophysics*, *367*, 235–251.

Faulkner, D. R., T. M. Mitchell, J. Behnsen, T. Hirose, and T. Shimamoto (2011), Stuck in the mud? Earthquake nucleation and propagation through accretionary forearcs, *Geophys. Res. Lett.*, *38*, L18303, doi:10.1029/2011GL048552.

Frye, K. M., and C. Marone (2002), The effect of humidity on granular friction at room temperature, *J. Geophys. Res.*, *107*(B11), 2309, doi:10.1029/2001JB000654.

Gu, J. C., J. R. Rice, A. L. Ruina, and S. T. Tse (1984), Slip motion and stability of a single degree of freedom elastic system with rate and state dependant friction, *J. Mech. Phys. Solids*, *32*, 167–196.

Hayman, N. W., B. A. Housen, T. T. Cladouhos, and K. Livi (2004), Magnetic and clast fabrics as measurements of grain-scale processes within the Death Valley shallow crustal detachment faults, *J. Geophys. Res.*, *109*, B05409, doi:10.1029/2003JB002902.

Heaton, T. H. (1990), Evidence for and implications of self-healing pulses of slip in earthquake rupture, *Phys. Earth Planet. Inter.*, *64*, 1–20.

Ikari, M., C. Marone, and D. M. Saffer (2011), On the relation between fault strength and frictional stability, *Geology*, *39*, 83–86, doi:10.1130/G31416.

Johnson, P., B. M. Carpenter, M. Knuth, B. M. Kaproth, P.-Y. Le Bas, E. G. Daub, and C. Marone (2012), Nonlinear dynamical triggering of slow slip on simulated earthquake faults with implications to Earth, *J. Geophys. Res.*, *117*, B04310, doi:10.1029/2011JB008594.

Kaneko, Y., and J.-P. Ampuero (2011), A mechanism for preseismic steady rupture fronts observed in laboratory experiments, *Geophys. Res. Lett.*, *38*, L21307, doi:10.1029/2011GL049953.

Karner, S. L., and C. Marone (2001), Frictional restrengthening in simulated fault gouge: effect of shear load perturbations, *J. Geophys. Res.*, *106*, 19,319–19,337.

Kato, N., and T. E. Tullis (2001), A composite rate- and state-dependent law for rock friction, *Geophys. Res. Lett.*, *28*(6), 1103–1106, doi:10.1029/2000GL012060.

Lapusta, N., and J. R. Rice (2003), Nucleation and early seismic propagation of small and large events in a crustal earthquake model, *J. Geophys. Res.*, *108*(B4), 2205, doi:10.1029/2001JB000793.

Logan, J. M., M. Friedman, N. Higgs, C. Dengo, and T. Shimamodo (1979), Experimental studies of simulated fault gouges and their application to studies of natural fault zones, in *Analysis of Actual Fault Zones in Bedrock*, U.S. Geol. Surv. Open File Rep., *1239*, 305–343 .

Mair, K., and C. Marone (1999), Friction of simulated fault gouge for a wide range of velocities and normal stress, *J. Geophys. Res.*, *104*(B12), 28,899–28,914.

Marone, C. (1998), Laboratory-derived friction constitutive laws and their application to seismic faulting, *Annu. Rev. Earth Planet. Sci.*, *26*, 643–696.

Marone, C., and S. J. D. Cox (1994), Scaling of rock friction constitutive parameters: The effects of surface roughness and cumulative offset on friction of gabbro, *Pure Appl. Geophys.*, *143*, 359–386.

Marone, C., and B. Kilgore (1993), Scaling of the critical slip distance for seismic faulting with shear strain in fault zones, *Nature*, *362*, 618–622.

Marone, C., C. B. Raleigh, and C. H. Scholz (1990), Frictional behavior and constitutive modeling of simulated fault gouge, *J. Geophys. Res.*, *95*(B5), 7007–7025.

Marone, C., M. Cocco, E. Richardson, and E. Tinti (2009), The critical slip distance for seismic and aseismic fault zones of finite width, in *Fault-Zone Properties and Earthquake Rupture Dynamics*, Int. Geophys. Ser., vol. 94, edited by E. Fukuyama, pp. 135–162, International Geophysics, Academic Press, New York.

Mead, W. J. (1925), The geologic role of dilatancy, *J. Geol.*, *33*, 685–698.

Muhlhaus, H. B., and I. Vardoulakis (1987), Thickness of shear bands in granular materials, *Geotechnique*, *37*(3), 271–283.

Nagata, K., M. Nakatani, and S. Yoshida (2012), A revised rate- and state-dependent friction law obtained by constraining constitutive and evolution laws separately with laboratory data, *J. Geophys. Res.*, *117*, B02314, doi:10.1029/2011JB008818.

Nielsen, S., J. Taddeucci, and S. Vinciguerra (2010), Experimental observation of stick-slip instability fronts, *Geophys. J. Int.*, *180*, 697–702, doi:10.1111/j.1365-246X.2009.0444.x.

Niemeijer, A., C. Marone, and D. Elsworth (2010), Frictional strength and strain weakening in simulated fault gouge: Competition between geometrical weakening and chemical strengthening, *J. Geophys. Res.*, *115*, B10207, doi:10.1029/2009JB000838.

Niemeijer, A. C., and C. J. Spiers (2007), A microphysical model for string velocity weakening in phyollosilicate-bearing fault gouges, *J. Geophys. Res.*, *112*, B10405, doi:10.1029/2007JB005008.

Niemeijer, A. C., C. Marone, and D. Elsworth (2008), Healing of simulated fault gouges aided by pressure solution: results from rock analog experiments, *J. Geophys. Res.*, *113*, B04204, doi:10.1029/2007JB005376.

Noda, H., and T. Shimamoto (2010), A rate- and state-dependent ductile flow law of polycrystalline halite under large shear strain and implications for transition to brittle deformation, *Geophys. Res. Lett.*, *37*, L09310, doi:10.1029/2010GL042512.

Parsons, T. (2005), A hypothesis for delayed dynamic earthquake triggering, *Geophys. Res. Lett.*, *32*, L04302, doi:10.1029/2004GL021811.

Perrin, G., J. R. Rice, and G. Zheng (1995), Self-healing slip pulse on a frictional surface, *J. Mech. Phys. Solids*, *43*, 1461–1495.

Rabinowicz, E. (1958), The intrinsic variables affecting the stick–slip process, *Proc. Phys. Soc. London*, *71*, 668–675.

Rathbun, A. P., and C. Marone (2010), Effect of strain localization on frictional behavior of granular materials, *J. Geophys. Res.*, *115*, B01204, doi:10.1029/2009JB006466.

Rathbun, A. P., C. Marone, R. B. Alley, and S. Anandakrishnan (2008), Laboratory study of the frictional rheology of sheared till, *J. Geophys. Res.*, *113*, F02020, doi:10.1029/2007JF000815.

Rathbun, A. P., F. Renard, and S. Abe (2013), Numerical investigation of the interplay between wall geometry and friction in granular fault gouge, *J. Geophys. Res.*, *118*, 878–896, doi:10.1002/jgrb.50106.

Reynolds, O. (1885), On the dilatancy of media composed of rigid particles in contact, *Phil. Mag. S 5*, *20*, 469–481.

Rice, J. R. (1983), Constitutive relations for fault slip and earthquake instabilities, *Pure Appl. Geophys.*, *121*, 443–475.

Rice, J. R. (1993), Spatio-temporal complexity of slip on a fault, *J. Geophys. Res.*, *98*, 9885–9907.

Rice, J. R., and A. L. Ruina (1983), Stability of steady frictional slipping, *J. Appl. Mech.*, *105*, 343–349.

Rice, J. R., N. Lapusta, and K. Ranjith (2001), Rate and state dependent friction and the stability of sliding between elastically deformable solids, *J. Mech. Phys. Solids*, *49*, 1865–1898.

Richardson, E., and C. Marone (1999), Effects of normal force vibrations on frictional healing, *J. Geophys. Res.*, *104*, 28,859–28,878.

Rubin, A. M. (2008), Episodic slow slip events and rate-and-state friction, *J. Geophys. Res.*, *113*, B11414, doi:10.1029/2008JB005642.

Rubin, A. M. (2011), Designer friction laws for bimodal slow slip propagation speeds, *Geochem. Geophys. Geosyst.*, *12*, Q04007, doi:10.1029/1020GC003386.

Rubin, A. M., and J.-P. Ampuero (2005), Earthquake nucleation on (aging) rate-and-state faults, *J. Geophys. Res.*, *110*, B11312, doi:10.1029/2005JB003686.

Ruina, A. (1983), Slip instability and state variable friction laws, *J. Geophys. Res.*, *88*, 10,359–10,370.

Saffer, D. M., and C. Marone (2003), Comparison of smectite- and illite-rich gouge frictional properties: Application to the updip limit of the seismogenic zone along subduction megathrusts, *Earth Planet. Sci. Lett.*, *215*, 219–235.

Sammis, C. G., and R. L. Biegel (1989), Fractals, fault-gouge and friction, *Pure Appl. Geophys.*, *131*(1–2), 255–271.

Samuelson, J., D. Elsworth, and C. Marone (2009), Shear-induced dilatancy of fluid-saturated faults: Experiment and theory, *J. Geophys. Res.*, *114*, B12404, doi:10.1029/2008JB006273.

Samuelson, J., D. Elsworth, and C. Marone (2011), Influence of dilatancy on the frictional constitutive behavior of a saturated fault zone under a variety of drainage conditions, *J. Geophys. Res.*, *116*, B10406, doi:10.1029/2011JB008556.

Scholz, C. H. (2002), *The Mechanics of Earthquakes and Faulting*, 2nd ed., Cambridge Univ. Press, Cambridge, U. K.

Scott, D., C. Marone, and C. Sammis (1994), The apparent friction of granular fault gouge in sheared layers, *J. Geophys. Res.*, *99*(B4), 7231–7247.

Segall, P., and J. R. Rice (1995), Dilatancy, compaction, and slip instability of a fluid infiltrated fault, *J. Geophys. Res.*, *100*, 22,155–22,173.

Segall, P., A. M. Rubin, A. M. Bradley, and J. R. Rice (2010), Dilatant strengthening as a mechanism for slow slip events, *J. Geophys. Res.*, *115*, B12305, doi:10.1029/2010JB007449.

Sibson, R. H. (2003), Thickness of the seismic slip zone, *Bull. Seismol. Soc. Am.*, *93*(3), 1169–1178.

Sleep, N. H. (2005), Physical basis of evolution laws for rate and state friction, *Geochem. Geophys. Geosyst.*, *6*, Q11008, doi:10.1029/2005GC000991.

Sleep, N., E. Richardson, and C. Marone (2000), Physics of friction and strain rate localization in synthetic fault gouge, *J. Geophys. Res.*, *105*, 25,875–25,890.

Tesei, T., C. Collettini, B. Carpenter, C. Viti, and C. Marone (2012), Frictional strength and healing behaviour of phyllosilicate-rich faults, *J. Geophys. Res.*, 117, B09402, doi:10.1029/2012JB009204.

Tordesillas, A., J. F. Peters, and B. S. Gardiner (2004), Shear band evolution and accumulated microstructural development in Cosserat media, *Int. J. Num. Anal. Methods Geomech.*, *28*, 981–1010, doi:10.1002/nag.343.

Tullis, T. E., and J. D. Weeks (1986), Constitutive behavior and stability of frictional sliding of granite, *Pure Appl. Geophys.*, *124*, 383–414.

Ziv, A., and A. M. Rubin (2003), Implications of rate-and-state friction for properties of aftershock sequences: Quasi-static inherently discrete simulations, *J. Geophys. Res.*, *108*(B1), doi:10.1029/2001JB001219.

Zoback, M., S. Hickman, and W. Ellsworth (2010), Scientific drilling into the San Andreas fault zone, *Eos. Trans. AGU*, *91*(22), 197–199.